The 2010 IEEE/RSJ International Conference on
Intelligent Robots and Systems
October 18-22, 2010, Taipei, Taiwan

Micro/Nano Displacement Sensor for Piezoelectric Actuator with Multi-Stage Expansion Mechanism

Yong Yu, IEEE Member, Bo Song, IEEE Student Member, Renbing Chen, and Yunjian Ge

Abstract – **In this paper, a micro/nano displacement sensor for PZT actuator which could measure the minute displacement in micron or nanometer level has been proposed. This paper focus on the whole process of this novel sensor from the working principle, parameter determination to the FEM simulation and so forth. This sensor can enlarge the displacement of the PZT by utilizing the lever principle and the strain gauges can perceive the variation without amplifying the noise. About this sensor, we also use the flexure hinges as the rotation joints to obtain the expansion. In addition, we provide the accurate model for this special kind of displacement sensor, and through that people could design and set every parameter freely. Whatever the simulation results in FEM or the experiment data, both of which show that the sensor can perceive the displacement of the PZT actuator in micro/nano scale. Also, the characteristic experiment shows that the proposed sensor has a better performance such as higher level linearity, resolution than its former two generations.**

Index Terms – Micro/nano displacement sensor*; *Mathematic model, Flexure hinges*; *Strain gauges*; *Displacement expansion

I. INTRODUCTION

Piezoelectric actuator (PZT hereafter) has some advantages such as higher stiffness, faster response and smaller volume, all of which make it widely used in many micro/nano driving and location system, for instance, micro worktable, AFM (Atomic Force Microscope) [1], fluid control value and acoustical transducer. However, it still has several obvious disadvantages of which the most are hysteresis and nonlinear [2], so that the displacement measurement of PZT is required for PZT position control.

Various displacement measurements have been already used for acquiring the information of micro displacement [3][4][5]. Some of the measurement, for instance, laser interferometer with the optical principle need large space to fix, and couples of conventional measurements are not useful without an electric amplifier.

In this research, we consider utilizing the PZT's high stiffness to develop a displacement sensor for PZT. This sensor has multi-stage enlarger configuration in order to acquire a larger expansion ratio, and transfer the expanded displacement into the elastic body in which the strain gauges could measure the change of deformation. With the output of strain gauges we could acquire the displacement information input by PZT. The PZT displacement sensor will be used for PZT position control, in order to solve the hysteresis and nonlinear which influence the performance of micro/nano PZT actuator system.

In our research group, we have designed and fabricated two generations of this displacement sensor. Our first generation micro/nano-displacement sensor was unveiled in 2008 [6] which offered a measurement range of ±5 [μm], with resolution of 25 [nm] and its total size is only 38×38×38 [mm].The first prototype has already testified our theory of mechanical extension through flexure hinges. The sensor can measure the micro displacement linearly with low error. The stiffness, distribution of the strains and the expansion ratio are computed either by the theory or the FEM simulations. The static displacement experiments were carried out from which the performance of the sensor is almost uniform to simulation result.The mechanical configuration of the displacement sensor in this research is consist of some levers and hinges, where the levers could offer high stiffness as well as the function of displacement expansion [7] that is also the essential point to this sensor.

This research considers using flexure hinges to solve these above problems [8][9][10]. Using flexure hinge mechanisms can meet the requirements of high precision [11]. Flexure hinges gain their mobility from an elastic and plastic deformation exclusively. To achieve a high life cycle the deformation should be remained in the elastic strain. Fig. 1 shows a conventional flexure hinge, a cantilever beam with a circular notch, where the deformations will take place nearly only at the point of the smallest cross-section [12].

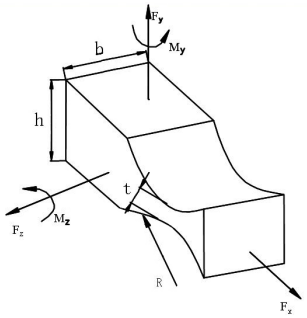

Fig.1 Uniaxial flexure hinge

In the next generation, we optimized the total configuration as well as added more powerful process circles. All of these improvements help this third generation sensor to promote its resolution.This third generation micro/nano displacement sensor provides superior sensitivity and nano-level resolution

Yong Yu is with Graduate School of Science and Engineering, Kagoshima University, Kagoshima 890-0065, Japan, yu@mech.kagoshima-u.ac.jp

Bo Song is with ECE Department, Michigan State University, East,Lansing, MI, US, song2006@mail.ustc.edu.cn.

Renbing Chen is with Institute of Intelligent Machine, Chinese Academy of Sciences, Hefei, Anhui Province, China and Department of Automation, University of Science and technology of China, Hefei, Anhui Province, China, pinghu@mail.ustc.edu.cn

Yunjian Ge is with Institute of Intelligent Machine, Chinese Academy of Sciences, Hefei, Anhui Province, China, yjge@iim.ac.cn

5[nm] with simple structure and a minute nonlinearity in the working range.

II. Configuration and Principle of Third Generation Micro/Nano Displacement Sensor

A. Working principle

Normally, the destination of the mechanical expansion is to enlarge the displacement of PZT with the principle of lever mechanism. The ratio of magnification is essential to the whole configuration. Though the expansion ratio would be the larger the better, considering the size of the sensor body, we cannot pick up a huge ratio for the reason that we should fix the PZT actuator inside the sensor tightly, as well as make sure the whole size is under control to be a smaller one which could be fixed in micro worktable. Thus, we still choose multi-steps expansion just like Fig.3 shows, where several levers and hinges are utilized to construct a lever-hinge displacement expansion mechanism.

The input displacement is imported at the hinge of B, and rotates lever AB' and B'C where two parts could be regarded as a one-lever rigid AC (see Fig.3(B)) around hinge A, and the output displacement of hinge C is enlarged through the lever AC. This is the first enlarger stage. Simultaneously, relatives to lever DE we used CE as a transition lever. Hinge C could also be seemed as the input point of displacement which makes lever CE to rotate around the hinge C. Finally hinge E provides the input displacement to lever DE as well as the expanded displacement provides the output displacement of the upper end in elastic body FG which is a rather thin flake. That is the second expansion stage. With limited DOF of lower end of the elastic body G which could be bent and acquire the topmost surface strain in the each end of elastic body and with the help of strain gauge pasted in the surface, we could finally gain the perception of elastic body's deformation which could reflect the input displacement by compute the expansion ratio of the whole system.

B. The Configuration of the Sensor

As is shown in Fig.2, the figuration of the sensing element for the displacement sensor is composed of a monolithic cube shell in which we cave the hinges, members as well as the elastic body through the wire cutting technology. Posing a PZT inside the sensor, simultaneously holding the upper surface of the PZT connected firmly with roof of sensor, we can acquire the displacement information by the roof which is a solo axis displacement. By a series of members and flexure hinges in the surface of the sensor the micro displacement can be enlarged and transferred to the elastic body. Here, we use the flexure hinges not only as the displacement amplified tool but as energy storage cells by using which the deformation could be resumed immediately when the displacement is given by the PZT dismiss, and without which the sensor would not operate in real time. Consequently, the measure sensitivity and the real time response of the sensor are increased.

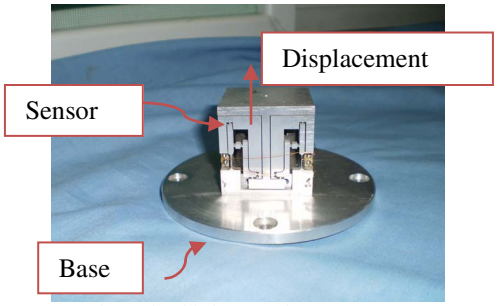

Fig.2 The third generation sensor

C. Expansion ratio

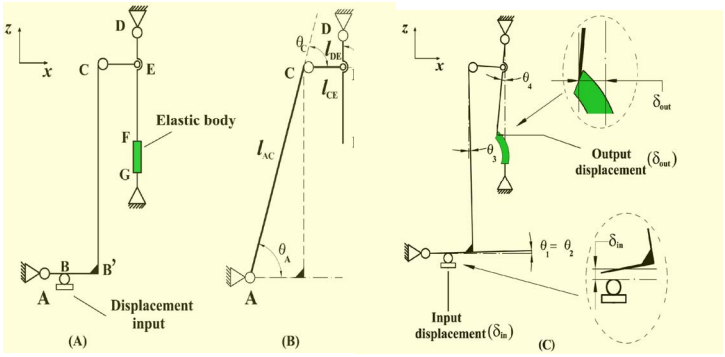

Fig.3 Lever-hinge displacement expansion mechanism

In order to calculate total extension ratio of the sensor, we set some parameters to the levers shown by Fig.3(A), l_{AB}= 2.14[mm], $l_{BB'}$=2.63[mm], $l_{B'C}$=14.1[mm], l_{CE} =1.90[mm], l_{ED}=8.30[mm]. We simplify this figuration as a traditional four-bar linkage section (see Fig.3(B)) for obtaining kinematics equation.

In Fig.3(B), we set $[x_A, y_A]^T$, $[x_C, y_C]^T$, $[x_E, y_E]^T$ and $[x_D, y_D]^T$ as the position vectors of joint A, C, E and D, l_{AC}, l_{CE}, l_{DE} as the length of each lever, and θ_A, θ_B, θ_C, θ_D, θ_E as the rotational angle of hinge A, B, C, D and E. We have

$$\begin{bmatrix} x_C \\ y_C \end{bmatrix} = \begin{bmatrix} x_A + L_{AC}\cos\theta_A \\ y_C + L_{AC}\sin\theta_A \end{bmatrix}, \tag{1}$$

$$\begin{bmatrix} x_E \\ y_E \end{bmatrix} = \begin{bmatrix} x_C + L_{CE}\cos(\theta_C + \theta_A) \\ y_C + L_{CE}\sin(\theta_C + \theta_A) \end{bmatrix}, \tag{2}$$

$$\begin{bmatrix} x_D \\ y_D \end{bmatrix} = \begin{bmatrix} x_E + L_{ED}\cos(\theta_A + \theta_C + \theta_E) \\ y_E + L_{ED}\sin(\theta_A + \theta_C + \theta_E) \end{bmatrix}. \tag{3}$$

Then we get the expression of x_D and y_D

$$\begin{bmatrix} x_D \\ y_D \end{bmatrix} = \begin{bmatrix} x_A + L_{AC}\cos\theta_A + L_{CE}\cos(\theta_C + \theta_A) + L_{ED}\cos(\theta_A + \theta_C + \theta_E) \\ y_A + L_{AC}\sin\theta_A + L_{CE}\sin(\theta_C + \theta_A) + L_{ED}\sin(\theta_A + \theta_C + \theta_E) \end{bmatrix}. \tag{4}$$

After the differential process, we get

$$\begin{bmatrix} -L_{AC}S_A - L_{CE}S_{AC} - L_{ED}S_{ACE} & l_{AC}C_A + L_{CE}C_{AC} + L_{ED}C_{ACE} \\ 0 & 0 \\ -L_{ED}S_{ACE} & L_{ED}C_{ACE} \\ 0 & 0 \\ -L_{CE}S_{AC} - L_{ED}S_{ACE} & L_{CE}C_{AC} + L_{ED}C_{ACE} \end{bmatrix}^T \begin{bmatrix} \Delta\theta_A \\ \Delta\theta_B \\ \Delta\theta_C \\ \Delta\theta_D \\ \Delta\theta_E \end{bmatrix} = \begin{bmatrix} \Delta x_D \\ \Delta y_D \end{bmatrix}, \tag{5}$$

where S_A, S_C, S_E, S_{AC}, S_{ACE} denote $\sin\theta_A$, $\sin\theta_C$, $\sin\theta_E$, $\sin(\theta_A+\theta_C)$, $\sin(\theta_A+\theta_C+\theta_E)$; C_A, C_C, C_E, C_{AC}, C_{ACE} denote $\cos\theta_A$, $\cos\theta_C$, $\cos\theta_E$, $\cos(\theta_A+\theta_C)$, $\cos(\theta_A+\theta_C+\theta_E)$ respectively for simple. $\Delta\theta_A$, $\Delta\theta_B$, $\Delta\theta_C$, $\Delta\theta_D$, $\Delta\theta_E$ are the angle displacement

of θ_A, θ_B, θ_C, θ_D, θ_E. In Fig.3(C), we use θ_1, θ_2, θ_3, θ_4, denote $\Delta\theta_A$, $\Delta\theta_B$, $\Delta\theta_D$ and $\Delta\theta_E$. Since $\Delta x_D = 0$, $\Delta y_D = 0$, we have

$$\begin{bmatrix} -L_{AC}S_A - L_{CE}S_{AC} - L_{ED}S_{ACE} & L_{AC}C_A + L_{CE}C_{AC} + L_{ED}C_{AC} \\ 0 & 0 \\ -L_{ED}S_{ACE} & L_{ED}C_{ACE} \\ 0 & 0 \\ -L_{CE}S_{AC} - L_{ED}S_{ACE} & L_{CE}C_{AC} + L_{ED}C_{ACE} \end{bmatrix}^{\mathrm{T}} \begin{bmatrix} \Delta\theta_A \\ \Delta\theta_B \\ \Delta\theta_C \\ \Delta\theta_D \\ \Delta\theta_E \end{bmatrix} = \begin{bmatrix} 0 \\ 0 \end{bmatrix}. \quad (6)$$

We set the initial parameters as below,

$L_{AC} = 14.7[\mathrm{mm}]$, $L_{CE} = 1.9[\mathrm{mm}]$, $L_{ED} = 8.3[\mathrm{mm}]$,

$\theta_A = 73.3[\mathrm{deg}]$, $\theta_C = 0[\mathrm{deg}]$, $\theta_E = 90[\mathrm{deg}]$.

Accordingly, we obtain the expression from (6) as

$$\begin{bmatrix} -18.285 & 0 & -2.385 & 0 & -4.205 \\ -3.180 & 0 & -7.950 & 0 & -7.404 \end{bmatrix} \begin{bmatrix} \Delta\theta_A \\ \Delta\theta_B \\ \Delta\theta_C \\ \Delta\theta_D \\ \Delta\theta_E \end{bmatrix} = \begin{bmatrix} 0 \\ 0 \end{bmatrix}, \quad (7)$$

$$\begin{bmatrix} \Delta\theta_C \\ \Delta\theta_E \end{bmatrix} = \begin{bmatrix} 7.736 \\ -8.736 \end{bmatrix} \Delta\theta_A. \quad (8)$$

Thereby, the output displacement in Fig. 3(C) is

$$\delta_{out} = \Delta\theta_E L_{DF} = 8.136 \Delta\theta_A L_{DF}. \quad (9)$$

$\Delta\theta_A$ is a rather micro displacement angle that could be closely equal to the value of $\tan\Delta\theta_A$, moreover

$$\Delta\theta_A \approx \tan\Delta\theta_A = \frac{\delta_{in}}{L_{AB}}. \quad (10)$$

Therefore, we have $\delta_{\mathrm{in}} = \Delta\theta_{\mathrm{A}}$, and finally the total expansion ratio K_1 of the lever-hinge expansion mechanism can be expressed as

$$K_1 = \left| \frac{\delta_{out}}{\delta_{in}} \right| = 44.9. \quad (11)$$

Then, we regard the elastic body FQ as a thin flake. Based the material mechanics of bending deformation, when we set the input displacement as 5 [μm], we could obtain the maximum strain in the surface. For simple, we consider this elastic body only has a tensile deformation and the total length of FQ could be calculated as

$$L_{TFQ} = \sqrt{L^2_{FQ} + \delta^2_{out}} = 5.53455\ [\mathrm{mm}]. \quad (12)$$

Then the strain of elastic body is

$$\varepsilon = \frac{L_{TFQ} - L_{FQ}}{L_{FQ}} = 8.2278 \times 10^{-4}. \quad (13)$$

The above analysis is based on the assumption that all the levers are rigid bodies which means there is no deformation happened when they transmit force or torque.

III. Accurate Model Analysis

A. The hinges

The previous computation is based on that the all the levers are rigid and all the hinges are common ones. However, normally, the lever would happen material deformation whatever the material we used, and in addition, the hinges we used here are flexure hinges which would preserve energy when they have rotation. This is quite different from common hinges. It is very essential to built up an accurate model that put the material deformation and flexure hinges in thought and based on which we could find out the precisely extension ratio. Moreover, this model would help us to set every parameter freely in designing configuration for new sensor.

Fig.1 shows the basic parameters of the uniaxial flexure hinge. The moment M_Z brings the deflection angle α_Z about Z axis of the uniaxial flexure hinge, and the relationship [13] between them is

$$\frac{\alpha_z}{M_Z} = \frac{3}{2EbR^2}\left[\frac{1}{2\beta+\beta^2}\right]\left\{\left[\frac{1+\beta}{\gamma^2} + \frac{3+2\beta+\beta^2}{\gamma(2\beta+\beta^2)}\right]\left[\sqrt{1-(1+\beta-\gamma)^2}\right] + \left[\frac{6(1+\beta)}{(2\beta+\beta^2)^{3/2}}\right]\left[tg^{-1}\left(\sqrt{\frac{2+\beta}{\beta}} \times \frac{\gamma-\beta}{\sqrt{1-(1+\beta-\gamma)^2}}\right)\right]\right\}, \quad (14)$$

where $\beta = t/2R$, $\gamma = t/2R$, E is the elastic modulus of the material and b is the thickness of the hinge. This expression is so complex that we seldom use. Instead, we simplify that expression into a simple form [12] as

$$\frac{1}{\rho} = \frac{\frac{d^2y}{dx^2}}{\left[1 + \left(\frac{dy}{dx}\right)^2\right]^{3/2}}, \quad (15)$$

where ρ is the curvature radius.

The travel of this sensor is rather small, and when the deformation happens, deflection is far more beyond the total length of the hinge. For the reasons above, we get

$$\frac{dy}{dx} << 1, \quad (16)$$

$$\frac{1}{\rho} = \frac{d^2y}{dx^2}. \quad (17)$$

In the condition of the small angle of rotation, we can use $\theta \approx \tan\theta = dy/dx$, and converse the rectangular coordinate to polar coordinates, then the angle of rotation of flexure hinge can be expressed as

$$\theta = \int_0^{\pi} \frac{12MR\sin\alpha}{Eb(2R + t - 2R\sin\alpha)^3} d\alpha. \quad (18)$$

R and t are the crucial parameters of the hinge. Giving a great value of t and a small value of R, the stiffness, dynamic performance and anti-interference properties are superior. On the contrary, the sensitivity and resolution are splendid when t is bigger and R is smaller. It is a dilemma. Our sensor is working for measuring the micro displacement and force not for transmission. Consequently, it is vital to ensure the sensitivity and resolution of the sensor, for which we choose to increase R and decrease t, simultaneously considering the response frequency which also restricts R, in addition the thickness of the hinge should be more than 0.3[mm] because of the wire cutting process, we choose 0.5[mm] as the value of parameter t, 3[mm] as the value of parameter b.

B. Mathematic modelling

When we fabricated the former two generations of sensor, we found that our theory model which is related in the last chapter is not as accurate as it was. This is because the deformation of material in every lever decreases the extension ratio of the total system, and does not match the results of FEM

simulation and experiment. In this chapter, we research on a new and more accurate model which has already put the material deformation in thought. Firstly, we decompose the total configuration into six sections and then we analyze each part's force and moment condition, balance, deformation as well as energy equations.

{1} Modelling analysis of lever PQ

In Fig.4, the lever PQ has suffered an input force *Fp* at point P and from that we could build up force and moment equation as following

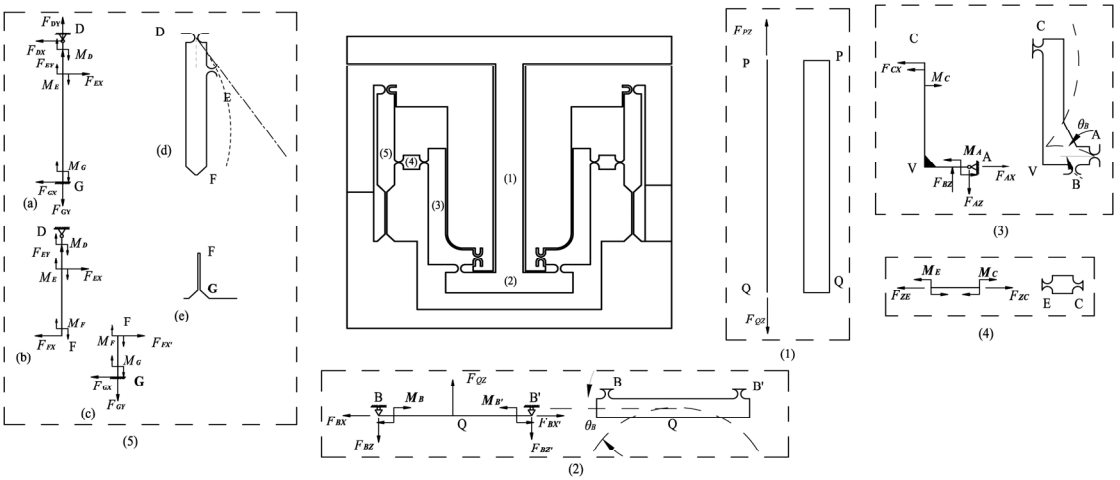

Fig.4 The decomposition structure of the sensor's configuration

As soon as the lever PQ transfers the F_{PZ} to next lever, it has a material deformation and according to the material mechanics, we could compute this deformation (S_{PQ}) through expression followed,

$$S_{PQ}=2F_{in1}L_{PQ}/Eb_{PQ}h_{PQ}. \tag{23}$$

S_{PQ} is the material deformation of lever PQ along Z axis. L_{PQ}, b_{PQ} and h_{PQ}, are the length, width and height of lever PQ respectively. E is the elastic modulus of material, and E=200Gpa. Therefore, the output displacement at point Q is

$$S_{outQ}= S_{intotal}-S_{PQ}. \tag{24}$$

$S_{intotal}$ is the input displacement of the sensor. Also the deformation energy in of lever PQ could be computed as

$$En_1=2F_{in1}S_{PQ}/2=F_{in1}S_{PQ}. \tag{25}$$

{2} Modelling analysis of lever BQ

The lever BQ has suffered five force and two moments simultaneously and from that we could build up force and moment equation as following,

$$\sum F_2=0, \tag{26}$$

$$\sum M_2=0. \tag{27}$$

Then we get

$$F_{BZ}= F_{BZ'} =F_{QZ}= F_{in1}, \tag{28}$$

$$F_{BX}= F_{BX'}, \tag{29}$$

$$M_B= M_{B'}, \tag{30}$$

$$M_B=K(\theta_A+\theta_B), \tag{31}$$

where θ_A(in Fig.4) and θ_B denote the rotation angles of lever AV and lever BB', K is the angle stuffiness of flexure hinge. The lever BB' has surfer both a force F_{QZ} and two moments $M_B= M_{B'}$ all of which form the material deformation of lever

$$\sum F_{z1}=0, \tag{19}$$

$$\sum M_1=0. \tag{20}$$

From eq. (19) we get

$$F_{QZ}= F_{PZ}. \tag{21}$$

Here we use F_{in1} to denote half of total input force F_{PZ}, so that

$$F_{QZ}= 2F_{in1}. \tag{22}$$

BB', in addition this total deformation of lever BB' could be decompose as two parts W_{QBT} and W_{QBF},

$$W_{QB}=W_{QBF}+W_{QBT}, \tag{32}$$

$$W_{QBF}=F_{in1}L^3_{BB'}/4Eb_{QB}h^3_{QB}, \tag{33}$$

$$W_{QBT}=M_BL^2_{BB'}/48Eb_{QB}h^3_{QB}, \tag{34}$$

where W_{QBT} and W_{QBF} denote the material deformation caused by force and moment. Since

$$\theta_B=W_{QB}/L_{QB}, \tag{35}$$

we can obtain Mb and θ_B from eqs. (31) and (35)

$$\theta_B=\frac{2(-2F_{in1}KL_{BB}L_{PQ}+4b_{PQ}F_{in1}h_{PQ}L_{AB}L^2_{BB}E+b_{PQ}h_{PQ}KL_{BB}S_{\text{intotal}}E)}{b_{PQ}h_{PQ}E(-2KL_{AB}L_{BB}+KL^2_{BB}+16b_{BQ}h^3_{BQ}L_{AB}E)}, \tag{36}$$

$$M_B=\frac{4(2b_{PQ}F_{in1}h_{PQ}KL^2_{BB}L_{AB}-4b_{PQ}F_{\text{in1}}h_{PQ}KL^3_{BB}}{b_{PQ}h_{PQ}(-2KL_{AB}L_{BB}+KL^2_{BB}+16b_{BQ}h^3_{BQ}L_{AB}E)}-\frac{-8b_{BQ}F_{in1}h^3_{BQ}KL_{AB}+4b_{PQ}b_{BQ}h_{BQ}h^2_{PQ}KS_{\text{intotal}}E)}{b_{PQ}h_{PQ}(-2KL_{AB}L_{BB}+KL^2_{BB}+16b_{BQ}h^3_{BQ}L_{AB}E)}. \tag{37}$$

Therefore, the output displacement of point B could be expressed as

$$S_{outB}=S_{outQ}-W_{QB}. \tag{38}$$

Also the deformation energy of lever BQ could be computed as

$$En_2=\frac{W_{QB}F_{in1}}{4}+\frac{K\theta^2_B}{2}+\frac{M\theta_B}{2}. \tag{39}$$

{3} Modelling analysis of lever DF

In order to deal with these two complex parts both of which have suffered various forces and moments, we first analysis

these two part as a whole structure and then decompose it. In Fig.4(5)(a), the lever DG has suffered two force and two moments simultaneously and from that we get

$$F_{EX}\text{-}F_{DX}\text{-}F_{GX}=0, \tag{40}$$

$$F_{DY}+F_{GY}\text{-}F_{EY}=0, \tag{41}$$

$$F_{EX}L_{DE}\text{-}M_D\text{-}M_E\text{-}M_G\text{-}F_{GX}L_{DG}=0. \tag{42}$$

Also, when we decompose this whole lever DG into lever DF and lever FG, we can build couples of new equations. In Fig.4(5)(c), the force and moment equations could be built as

$$F_{DX}+F_{FX}\text{-}F_{EX}=0, \tag{43}$$

$$F_{EX}L_{DE}\text{-}M_D\text{-}M_F\text{-}F_{FX}\text{-}L_{DF}=0. \tag{44}$$

Finally, in the last part of the sensor lever FG, we could get another two equations, they are

$$F_{FX}= F_{GX}, \tag{45}$$

$$F_{FX}\cdot L_{FG}+M_F\text{-}M_G=0. \tag{46}$$

Though solving the equations from (55) to (61), we could get the expression of

$$M_F=F_{EX}L_{DE}-M_D-\frac{L_{DE}M_E}{L_{DF}-L_{DG}-L_{FG}}, \tag{47}$$

$$M_G=F_{EX}L_{DE}-M_D-M_E-\frac{L_{DG}M_E}{L_{DF}-L_{DG}-L_{FG}}, \tag{48}$$

$$F_{DX}=F_{EX}-\frac{M_E}{L_{DF}-L_{DG}-L_{FG}}, \tag{49}$$

$$F_{GX}=\frac{M_E}{L_{DF}-L_{DG}-L_{FG}}, \tag{50}$$

$$F_{FX}=-\frac{M_E}{L_{DF}-L_{DG}-L_{FG}}, \tag{51}$$

The lever DF has surfer both a force F_{GZ} and a moments both of which form the material deformation of lever DF, in addition this total deformation of lever DF could be decompose as two parts, W_{DFT} and W_{DFF},

$$W_{DF}=W_{DEF}+W_{DET}+W_{DFF}+W_{DFT}, \tag{52}$$

$$W_{DEF}=F_{EX}L_{DE}^2(3L_{DF}-L_{DE})/(6EI_{DF}), \tag{53}$$

$$W_{DFF}=F_{FX}L_{DF}^3/(2EI_{DF}), \tag{54}$$

$$W_{DET}=-M_EL_{DE}(L_{DF}-L_{DE}/2)/EI_{DF}, \tag{55}$$

$$W_{DFT}=-M_FL_{DF}^2/2EI_{DF}, \tag{56}$$

$$\theta_{DFT}=M_FL_{DF}/EI_{DF}. \tag{57}$$

θ_{DFT} is the rotation angle of hinge F by the moment M_F and

$$I_{DF}=b_{DF}h_{DF}^3/12, \tag{58}$$

$$\theta_D=S_{outE}/L_{DE}. \tag{59}$$

So, the total output displacement of lever DF is

$$S_{outF}=W_{DE}+\frac{L_{DF}}{L_{DE}}S_{outE}. \tag{60}$$

Also the deformation energy of lever DF could be computed as

$$En_5=\frac{K\theta_D^2}{2}+\frac{F_{outE}W_{DEF}}{2}+\frac{M_E\theta_E}{2}+\frac{F_{FX}W_{DFF}}{2}+\frac{M_F\theta_{DFT}}{2}. \tag{61}$$

{4} Modelling analysis of lever FG

The lever FG has suffered a force and a moments both of which form the material deformation of lever FG , in addition this total deformation of lever FG (W_{FG}) could be decomposed as two parts, W_{FGT} and W_{FGF},

$$W_{FG}=W_{FGT}+W_{FGF}, \tag{62}$$

$$W_{FGF}=F_{FX}L_{FG}^3/(3EI_{FG}), \tag{63}$$

$$W_{FGT}=-M_FL_{FG}^2/2EI_{FG}, \tag{64}$$

$$\theta_{FGT}=M_FL_{FG}/EI_{FG}, \tag{65}$$

$$I_{FG}=b_{FG}h_{FG}^3/12. \tag{66}$$

Therefore, the total output displacement of lever FG is

$$S_{outF}=W_{FG}. \tag{67}$$

Also the deformation energy of lever FG could be computed as

$$En_6=\frac{F_{FX}W_{FGF}}{2}+\frac{M_F\theta_{QGT}}{2}. \tag{68}$$

Now, we have various equations as well as many parameters. We must select some useful parameters and their equations. In order to construct enough equations to solve the relationship between F_{in1}, $S_{intotal}$ and S_{outF} we must at least six equations and other three variables to deal with these embedded parameters.

First, we build an energy equation. The external force work of the whole sensor is

$$En_{out}=En_1+En_2+En_3+En_4+En_5+En_6, \tag{69}$$

where $En_{out}=2F_{in1}S_{intotal}$. Then we use force, moment and energy to build simultaneous equations and set F_{in1}, S_{outF}, θ_A, θ_C, θ_D, M_B as variables.

These equations are too large to give every one's full expression if we put all the equations together. So, the best way for this difficulty is to solve couples ratter simpler equations by means of valuation some of these parameters. After careful thought, we set some initial parameters.When we give the $S_{intotal}=5\times10^{-3}$ [mm], E=200Gpa and K=3.18, where E is the Elastic Modulus, K is the rotation stiffness of flexure hinge, we get the $S_{out}=4.283\times10^{-2}$ [mm] $F_{in1}=13.031$ [N], $F_{FX}=3.453\times10^{-2}$ [N], $M_F=9.361\times10^{-5}$ [Nm]. So the maximum stress of elastic body FG is

$$\sigma_{\max}=\frac{M}{W_Z}=\frac{M_{FG}}{\frac{b_{FG}E_{FG}^2}{6}}, \tag{70}$$

where W_Z is the section modulus in bending. Here, we consider that the elastic body FG has a bending deformation due to a moment M_F, and a force F_{FX} together.

$$\varepsilon_{\max}=\frac{\sigma_{\max}}{E}=\frac{M}{W_ZE}=\frac{M_F+F_{FX}\times L_{FG}}{\frac{b_{FG}h_{FG}{}^2E}{6}}=2.961\times10^{-4}. \tag{71}$$

IV. FEM SIMULATION

In order to select the appropriate position of each strain gauge and to give a scientific evaluation on measure sensitivity and of this sensor, it is very essential to realize the structural behaviour of the sensing element. The sensing element of the sensor is monolithic with a rather complicated configuration, thus it is hard to provide a pure theory accurately about the solid mechanics but to use the FEM

simulations (see Fig.5 and this deformation has been amplified 200 times) which can determine the strain distribution of the elastic body [14][15].

The finite element model is meshed with smart mesh division then refines the parts which we are interested in, for instance, the elastic body and flexure hinges. The material of the sensor is 35CrMnSiA, and its elastic modulus E=200×10^9 [Pa], Poisson's ratio μ = 0.28, density is 8.23 ×103 [kg/m^3]. The FEM simulations are implemented in the condition of that a displacement is applied to the roof of the sensor using which simulated the displacement of PZT which should be inside the sensor. The displacement applied in the analysis is S_Z =0.005[mm].

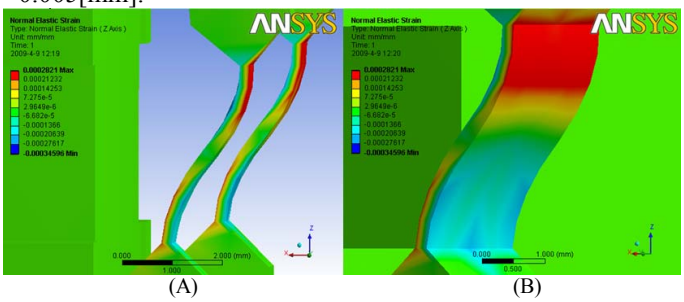

(A) (B)

Fig.5 The distribution of strain along Z-axis

Fig.5 shows the distribution of strain along Z-axis under the displacement along Z-axis S_Z=5[μm] of the elastic body in which we paste the strain gauges. There are both negative and positive strain parts in the same elastic body, which means the deformation of the body seems like the symbol S. From the positive part in the upper body to the negative part in the lower body the strain gradient has a perfect distribution. Furthermore in the back of the body the strain distribution is just opposite which means when the strain in one face of the body is positive, the other face of the elastic body do have the negative strain, and vice versa. Maximal positive strains (≈2.82×10^{-4}) and relative larger negative strains (≈ -2.52×10^{-4}) of the sensor happen in the each endpoint of the elastic body. These results are more superior compared to the former two generations (≈2.02×10^{-4}). Both of these results match the accurate theoretical model. Also the places where happen maximal positive and negative strains are the ones where the strain gauges are pasted.

V. Characteristic Experiments and Discussion

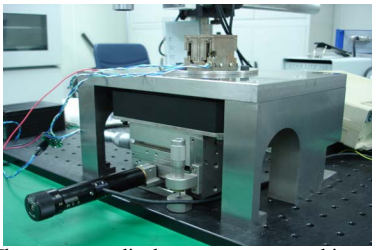

Fig.6 The prototype displacement sensor and its test platform

The prototype of this generation micro/nano displacement sensor (Fig.6) was manufactured according to the FEM model. A series of experiments have been done in order to evaluate the performance of the sensor. The displacement sensor was fixed on a calibration table which is consisted of a manual coarse adjustment table, an accurate nano-positioning table and data processing module. The resistance strain gauges which sensitivity coefficient is 2.0 we used here are pasted on the surfaces of elastic body where the maximum strain happened in our FEM simulation. DSP2812 system with signal pre-processing is also designed and set as a read-out device of the whole system (see Fig.7).

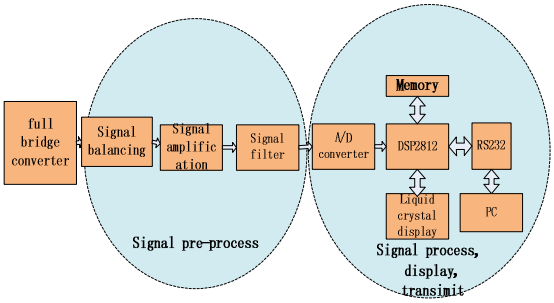

Fig.7 Schematic diagram of experimental

A. Static Performance

The whole process of calibration takes part in the overall measurement system based on the Nano-Positioning and Scanning System (P517) developed by PI Company in Germany and it is showed in Fig.6. The P517 provides a scan scale of 0.03[mm], the closed-loop resolution is 0.1[nm] and full–range repeatability is 5%. We use the P517 to provide the nano-scale displacement and read the value of voltage output of the sensor. Also, a fitting curve simultaneously is added in order to form a set of control, from which we can know that whether the linearity of the sensor is superior or not.

At the beginning of the static performance experiment (see Fig.8, for example), we set the sensor into an initial condition which already has a contact between the sensor and the P517, and then we load the displacement 50[nm] by 50[nm], finally up to the 1000[nm] which is a rather safe displacement to this sensor. Contemporarily, the output voltage value of sensor would show on the computer screen.

The nonlinear error is 3.48%, 3.03%, 10.97%, 17.53% and 27.77% from the interval scale of 100[nm], 50[nm], 25[nm], 10[nm] and 5[nm] with the total range of each process is 0~2000[nm], 0~1000[nm], 0~500[nm], 0~200[nm] and 0~100[nm] (see Fig.8). Here we also use the Product-moment correlation coefficient (R^2) to depict the degree of correlation. The test points would match the fitting curve perfectly if R^2 is getting close to the value of one. The resolution of the whole sensor could be reach as high as 5[nm]. Also we did the experiments to test the repeatability of our sensor (Fig.8). Through that we can find several times testing points distributed along the fitting curve with the error of 5.76%.

B. Sensor Performance Analysis

The calibration experiment is in the foundation of displacement input and the voltage output, and from which we could see that the nonlinearity usually happens in the initial steps of the measurement scale. Consequently, we could use the relative superior segment to measure the displacement. Taking the experiment with 5[nm] interval (see Fig.8(e)) as an

example, after remove the fifth and sixth points the nonlinear error could be decreased as low as 18.75%. Also this nonlinear phenomenon probably due to that the machining accuracy of the sensor and the location of strain gauge are not easy to achieve the design parameters accurately.

C. Analysis of Nonlinear Error and Noise

The calibration experiment was carried on under the condition of constant temperature ($24^{\circ}C$) and atmospheric pressure. In addition there was no vibration happened in our base of test platform, all of which mean that temperature and vibration are not the reason for nonlinear errors. Consequently, two main reasons caused nonlinear in this experiment are the output error of P517, and signal process circle noise. For an instance, P517 Nano-Positioning and Scanning System has an output error within ± 0.5 nm. Also, data processing circle has a static error of ±0.03% (full scale). Besides, another reason for the nonlinear error happening is the noise interference. How to promote the ability of noise reduction needs to be further considered. In addition, some details such as the configuration of elastic body and position of gauges still need to revise to obtain superior performance.

VI. Conclusions

A novel generation micro/nano displacement sensor using levers and flexure hinges and based on strain gauges is presented in this paper. Also the accurate mathematic model is built up and this model quite matches the results from the FEM simulation. In the elastic body of this generation sensor, both the maximal positive and negative strains are far more superior than the former two generation. The static displacement experiments were carried out from which the performance of the sensor is almost uniform to simulation result. This nano/micro displacement sensor provides superior sensitivity and nano-level resolution with simple structure and a minute nonlinearity in the working range. In addition, from the mathematic model, we could optimize the parameters of configuration to obtain more superior characteristic as well as promote the linearity, and that is our future work.

References

[1] G. Binnig, C. F. Quate and C. Gerber, "Atomic force microscope," *Physical Review Letters*, vol. 56, pp. 930-933, 1986.

[2] S. B. Jung and S. W. Kim, "Improvement of scanning accuracy of PZT piezoelectric actuators By Feedforward Model-Reference Control," *Precision Engineering-Journal of the American Society for Precision Engineering*, vol. 16, pp. 49-55, 1994.

[3] Y. Liu and T. Higuchi., "Precision Positioning Device Utilizing Impact Force of Combined Piezo-Pneumatic Actuator," *IEEE/ASME Transactions on Mechatronics*, vol. 6, pp. 467-473, 2001.

[4] E. K. Chan and R. W. Dutton, "Electrostatic micromechnical actuator with extended range of travel," *Journal of Microelectromech. System.* Vol. 9, pp. 321-328, Sept. 2000.

[5] Y. Yu, T. Ishitsuka and S. Tsujio, "Torque Sensing of Finger Joint Using Strain-Deformation Expansion Mechanism," *Procee. of IEEE International Conference on Robot and Automation*. vol. 2, pp. 1850-1856, 2003.

[6] B. Song, Y. Yu, W.-C. Yang and Y.-J. Ge, "Research of micro/nano displacement sensor for piezoelectric actuator", Proceeding of 2008 IEEE International Conference on Robotics and Biomimetics, pp. 276 – 281, 2009

[7] Y. Yu, T. Chaen and S. Tsujio, "High-Stiffness and High-Sensitivity 3-Axis Force Sensor Using Strain-deformation Expansion Mechanism," *Proceedings of IEEE International Conference on Intelligent Robots and Systems*. pp. 4417-4422, 2006.

[8] B. J. Yi and G. B. Chung, "Design and experiment of a 3-DOF parallel micromechanism utilizing flexure hinges," *Robotics and Automation, IEEE Transactions on Publication*. vol.19, No. 4, pp. 604-612, 2003.

[9] J. Schlick and D. Zuehlke, "Smart Tong Grippers for Micro-Parts," *Smart Sensors, Actuators, and MEMS, Proceedings of the SPIE.* Vol. 5116, pp. 220-228. 2003.

[10] K. Mizutani, T. Kawano, and Y. Tanaka, "A piezoelectric-drive table and its application to micro-grinding of ceramic materials," *Precision Engineering-Journal of the American Society for Precision Engineering*, vol. 12, pp. 219-226, 1990

[11] J. P. Bacher, S. Bottinelli, J. M. Breguet and R. Clavel, "Delta(3): design and control of a flexure hinges mechanism," *Microrobotics and Microassembly Iii.* vol. 4568, pp. 135-142, 2001.

[12] J. Hesselbach and A. Raatz, "Pseudo-elastic flexure-hinges in robots for micro assembly," *Microrobotics and Microassembly Ii*. vol. 4194, pp. 157-167, 2000.

[13] S.-F. Xue, Q.-X. Li. *Design of Precision instrumens*, Beijing Tsinghua publishing house, pp. 203-210, 1991. (*in Chinese)*

[14] M. Meng, Z.-C. Wu, Y. Yu, Y. Ge and Y.-J. Ge, "Design and characterization of a six-axis accelerometer," *Procee. of IEEE International Conference of Robotics and Automation,* pp. 2356-2361, 2005.

[15] Y. Li and Q. Xu, "Design and analysis of a totally decoupled flexure-based XY parallel micromanipulator," *IEEE Transactions on Robotics,* vol. 25, no. 3, pp. 645-657,2009.

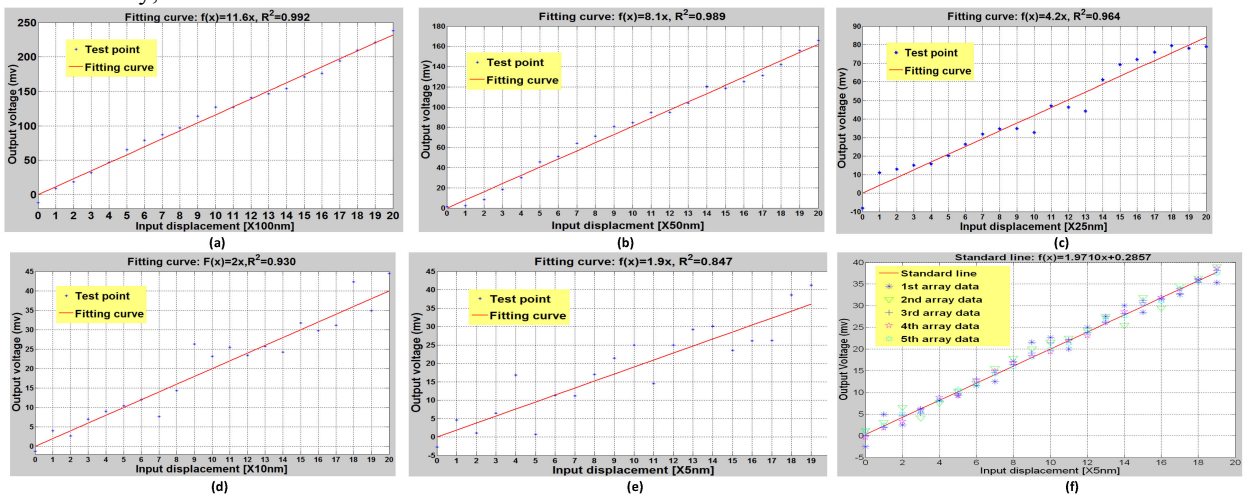

Fig.8 Experiment result and fitting curve. (a) for 100 [nm] interval; (b) for 50 [nm] interval; (c) for 25 [nm] interval; (d) for 10 [nm] interval; (e) for 5 [nm] interval ; (f) Test for repeatability